FIRST BEAM AT DARHT-II

Carl Ekdahl, E. O. Abeyta, L. Caudill, K. C. D. Chan, D. Dalmas, S. Eversole, R. Gallegos, J. Harrison, M. Holzscheiter, J. Johnson, E. Jacquez, B. Trent McCuistian, N. Montoya, K. Nielsen, D. Oro, L. Rodriguez, P. Rodriguez, M. Sanchez, M. Schauer, D. Simmons, H. V. Smith, J. Studebaker, G. Sullivan, C. Swinney, and R. Temple, LANL, Los Alamos, NM 87545, USA
Y. J. Chen, and T. Houck, LLNL, Livermore, CA 94551, USA
E. Henestroza, S. Eylon, W. Fawley, and S. S. Yu, LBNL, Berkeley, CA 94720, USA
H. Bender, W. Broste, C. Carlson, G. Durtschi, D. Frayer, D. Johnson, K. Jones, A. Meidinger, K. Moy, R. Sturgess, and C. Y. Tom, Bechtel Nevada, Los Alamos, NM 87544, USA
T. Hughes, and C. Mostrom, Mission Research, Albuquerque, NM 87110

Abstract

The second axis of the Dual Axis Radiographic Hydro-Test (DARHT) facility will provide up to four short (< 150 ns) radiation pulses for flash radiography of high-explosive driven implosion experiments[1]. To accomplish this the DARHT-II linear induction accelerator (LIA) will produce a 2-kA electron beam with 18-MeV kinetic energy, constant to within $\pm$ 0.5% for 2-μs. A fast kicker will cleave four short pulses out of the 2-μs flattop, with the bulk of the beam diverted into a dump. The short pulses will then be transported to the final-focus magnet, and focused onto a tantalum target for conversion to bremsstrahlung pulses for radiography. DARHT-II is a collaborative effort between the Los Alamos, Lawrence Livermore, and Lawrence Berkeley National Laboratories of the University of California.

INTRODUCTION

Commissioning of DARHT-II is proceeding in four phases. The first phase was a demonstration that the DARHT II technology could produce and accelerate a beam of electrons. Optimization of the injector and accelerator to produce a beam with the required final parameters and quality is the objective of the upcoming second phase of commissioning. The third phase will demonstrate the ability to produce multiple electron-beam pulses, and the final phase will demonstrate production of multiple-pulse radiographic-quality bremsstrahlung pulses.

DARHT-II was first turned on in early summer, 2002, and the first phase of commissioning is now complete. These tests were accomplished at reduced parameters to minimize risk of damage to this new accelerator. Table 1 shows the parameters for these experiments compared with the final parameters expected when all phases of commissioning are completed. We will detail some of the results from the first phase in this article.

ACCELERATOR

An 88-stage Marx generator that will produce a 3.2-MV output pulse that is flat for 2-μs powers the injector diode for DARHT-II. Because of the Marx risetime and the stray capacitances of injector structure, the risetime of this pulse at the diode is ~ 500 ns. To minimize risk of damage in the experiments reported here, the Marx generator was configured to produce a shorter, 1.2-μs FWHM pulse, which was even further shortened by using a crowbar switch on most shots.

A 16.5-cm diameter hot dispenser cathode in a shrouded Pierce-like diode produced a 1.2 –1.3-kA beam for the experiments reported here. The solenoidal magnetic-transport field is cancelled at the surface of the emitter with a bucking coil so that the (conserved) beam canonical angular momentum will be zero at the field-free bremsstrahlung converter, when installed.

After leaving the diode, the 3.0-MeV beam was accelerated by eight large-bore (36-cm diameter beam tube) induction cells to 4.2 MeV. The magnetic transport through these induction cells was tuned so that none of the off-energy electrons present in the ~500-ns beam head (produced by the diode-pulse risetime) executed betatron oscillations with amplitude greater than ¾ of the beam tube radius, thus keeping them well away from the accelerating gaps and insulators.

The beam next enters a special transport zone with a narrow energy bandpass to scrape off the long risetime, off-energy beam head. For these first experiments, this beam-head clean-up zone (BCUZ) was configured to pass the entire beam head during these initial tests, and the timing of the accelerator was set to accelerate the entire beam, including the rising portion of the pulse. The magnetic tune through the BCUZ compressed the beam to the smaller radius needed to match into the main accelerator.

After the BCUZ the beam enters the main accelerator, which consisted of 64 smaller-bore (25.4-cm diameter beam tube) "standard" induction cells for phase 1 experiments. Of these, two or three were inactive due to problems. The magnetic tune through the main accelerator gradually increased to a field of more than 1 kG on axis to suppress the beam-break-up (BBU) instability.

The magnetic tune for these experiments (Fig. 1) was designed using two beam dynamics codes [2]. First, the TRAK electron-gun design code [3] was used to establish initial conditions at the anode (initial radius, divergence, emittance) for the XTR envelope code [4] at the operating A-K potential of the diode. Then the tune was developed for the energy flattop of the beam using the accelerating voltages expected to be applied to the gaps. Finally, the

transport of the off-energy beam head was checked using XTR simulations in steps of 100-kV A-K potential, with initial conditions from individual TRAK simulations.

Table 1: DARHT-II Parameters

	These Experiments	**Final Parameters**
Beam Current	1.2-1.3 kA	2.0 kA
Pulse Length	0.5-1.2 µs (FWHM)	2.0 µs (FlatTop)
Diode	3.0 MeV	3.2 MeV
8 Injector Cells	1.2 MeV	1.4 MeV
Installed Standard Cells	64	70
Active Standard Cells	61-62	70
Exit Energy	12.5-12.7 MeV	18 MeV
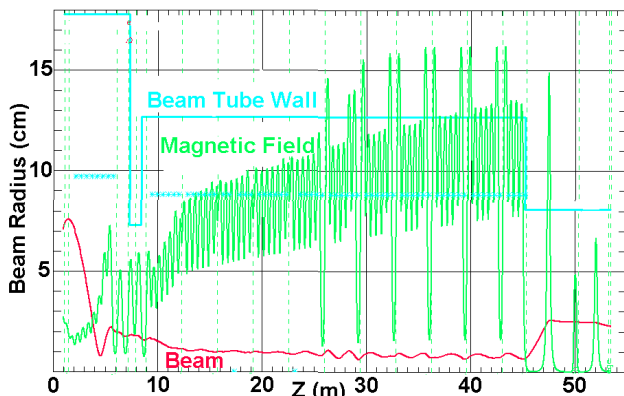
Figure 1. DARHT-II tune for commissioning experiments.

DIAGNOSTICS

DARHT-II is heavily instrumented with beam and pulsed-power diagnostics. In addition to diagnostics that monitor the Marx generator performance, there are capacitive dividers in the diode vacuum to measure the actual diode voltage waveform. Each induction cell has a resistive divider to measure the voltage waveform delivered by the PFN. There are beam position monitors (BPMs) at the entrance to each block of cells, as well as three more in the diode anode region, one at the exit of the injector cells, two in the BCUZ, and one just before the imaging target. For these experiments streak and framing cameras produced images of beam generated Cerenkov and optical transition radiation (OTR) light from targets inserted in the beam line. Finally, a magnetic spectrometer is used to measure the beam kinetic energy.

Diode Voltage Monitors

The A-K gap potential was measured using capacitive dividers. These monitors were 19-cm diameter plates positioned flush with the vacuum tank wall facing the diode cathode structure. Each monitor plate is integrated into a standard 45.7-cm vacuum port nipple. One of the monitors is recorded directly giving a signal proportional to dV/dt. This signal was integrated with software, and was calibrated against the beam energy measured with the magnetic spectrometer.

Beam Position Monitors

Each BPM consisted of an array of four B_θ-field detectors spaced 90° apart. Differencing the opposing detectors and normalizing to the sum of all four gave the position of the beam centroid with negligibly small errors [5]. Each detector was a (double-loop) balanced design with a Moebius crossover to minimize common mode signals arising from ground loops, radiation driven Compton currents, direct beam spill pickup, electric field pickup, and/or other interfering noise, EMP, or backgrounds. The loops were formed from SiO_2 insulated coax to maintain vacuum integrity and long term immunity to radiation backgrounds. Signals proportional to dB_θ/dt, were integrated and further processed in software to give beam current and centroid position. Calibration was accomplished in a "coaxial" test stand with an inner conductor that could be accurately offset from center. In addition to rigorous calibration, these BPMs have been checked against independently calibrated position monitors at the ETA, Thor, and DARHT-I accelerators.

Beam Imaging

Streak and framing cameras recorded images of beam generated Cerenkov and OTR light from targets inserted in the beam line at 45° to the axis. The targets were 0.3-mm thick SiO_2 wafers that were polished and aluminized on the front surface to produce OTR, and frosted on the back surface to scatter Cerenkov radiation into the line of sight orthogonal to the beamline. Target manipulation was accomplished by remote control from the control room.

The Bechtel/Nevada streak camera used a unique, anamorphic optical system that compressed the light in one dimension into a line that was imaged onto a coherent, linear fiber-optic array cemented to the remotely located camera. Two such arrangements provided simultaneous projections in the horizontal (X) and vertical (Y) directions, which were recorded on a 1024x1024 CCD readout camera. The anamorphic optical system simplified alignment, eliminated ambiguity resulting from beam motion, and eased analysis. Time-resolved moments and maximum-entropy reconstructions of the beam profile were obtained with analysis software (subject to the constraints of only two views) immediately after each shot.

The OTR angular distributions were recorded with a Bechtel/Nevada four-frame camera focused at infinity

through a large collection angle lens system. Another 1024x1024 CCD readout camera enabled immediate viewing and analysis of the data.

Spectrometer

A 45° sector magnet powered by a highly regulated supply is used to measure the energy of beam electrons passing through a 1-mm input collimator. The position of this beamlet in the momentum dispersion plane was registered with yet another Bechtel/Nevada streak camera with CCD readout. Light from a fast fluor in the momentum dispersion plane was focused onto a coherent fiber bundle that relayed it to the remotely located streak camera. This spectrometer system has been calibrated against an ion source, and has also been used to measure the energy of the DARHT-I and FXR (LLNL) beams.

RESULTS

A striking feature of this diode is the 7.8-MHz oscillation on the main pulse (Fig. 2 and Fig. 3), which is about $\pm1.5\%$ of the voltage at the peak. This is an LC oscillation caused by the capacitances and inductances of the injector structure. This LC oscillation damps out with a time constant of ~780 ns with no beam loading the diode. The decay time decreases as beam current loads the circuit. We varied the diode current by operating the cathode at temperatures below that required for space-charge limited emission. Oscillation damping-rate data acquired in those experiments imply that the decay time should be less than 250 ns when we operate at 2 kA. If so, the oscillation amplitude should decay to less than 0.3% by the time the voltage reaches its flattop value. In any case, a resistive damping circuit to further quench this oscillation is now being tested, and could be installed if necessary.

As shown in Fig. 4, the beam is accelerated by the eight injector cells without loss of current within the ~2% uncertainty of the measurement. Some of the beam head is then lost in the 15.2-cm diameter BCUZ throat (Fig. 5). Very little further loss occurs as the beam is accelerated through the remaining 64 accelerator cells (Fig. 6). These results verify that the magnetic tune indeed realized the design goal of negligible off-energy beam-head loss in the cells.
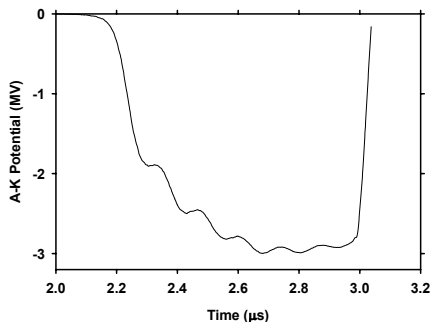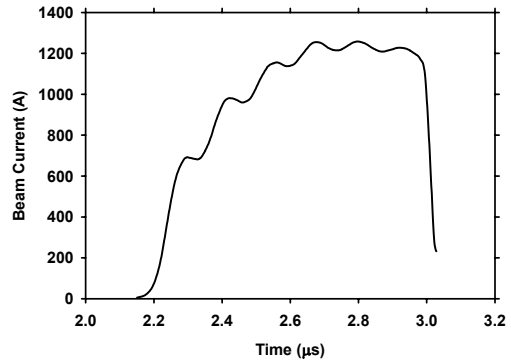

Figure 3. Electron beam current at diode exit.

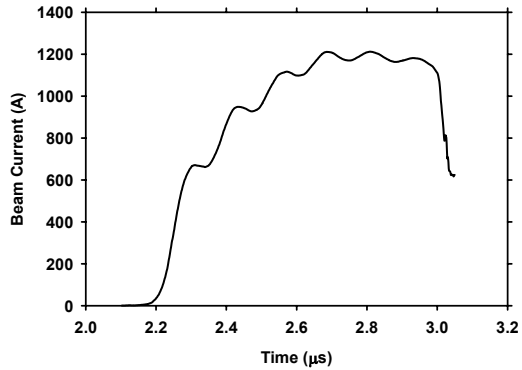Figure 4. Electron beam current at exit of injector cells.
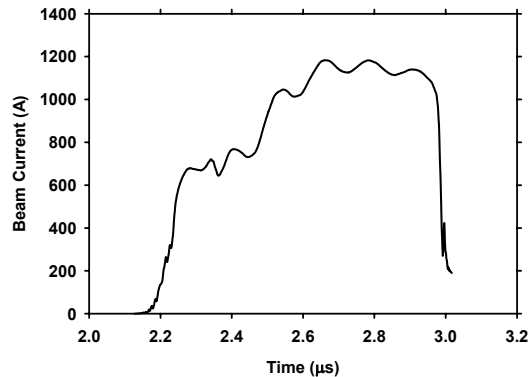
Figure 5. Electron beam current at BCUZ exit.
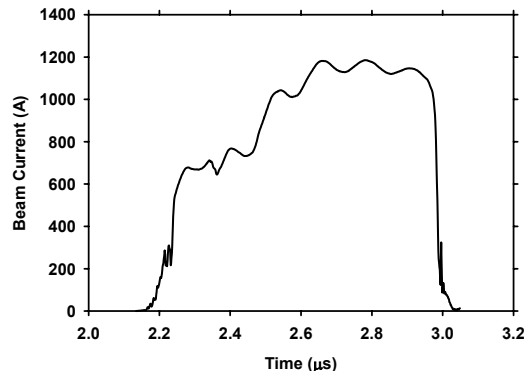

Figure 2. A-K gap potential.

Figure 6. Electron beam current at accelerator exit.

The ±1.5% beam energy oscillation in the diode causes an oscillation of the beam position as a result of an accidental magnetic dipole in the diode region. This is clearly evident at the first BPM, located at the diode exit (Fig. 7). This initial motion is modified by the magnetic transport, but does not grow in amplitude through the accelerator (Fig. 8). Although DARHT-II is equipped with steering dipoles throughout, they were neither needed nor used for these experiments.
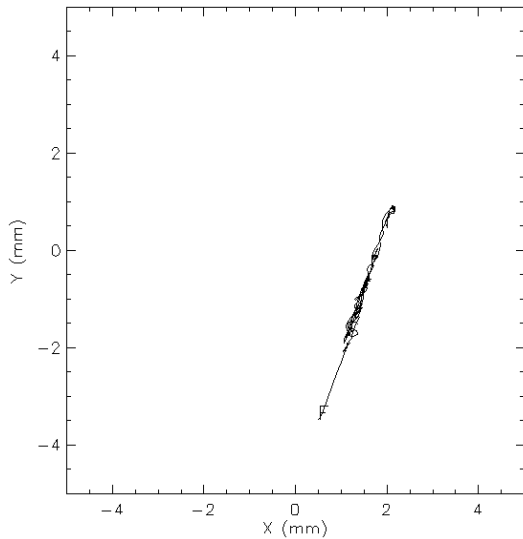

Figure 7. Beam position at diode exit during a 400-ns window around peak current. (S and F signify start and finish times).
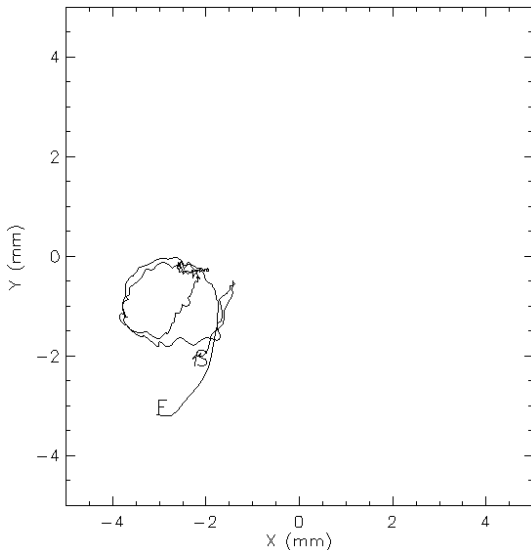

Figure 8. Beam position at accelerator exit during a 400-ns window around peak current. (S and F signify start and finish times).

The fully accelerated beam kinetic energy was measured with the magnetic spectrometer to be >12.2 MeV for 500 ns, with a peak energy >12.5 MeV (Fig. 9). The 7.8-MHz oscillations are clearly evident on this sensitive scale, although they amount to only ±0.4% of the accelerated beam energy.
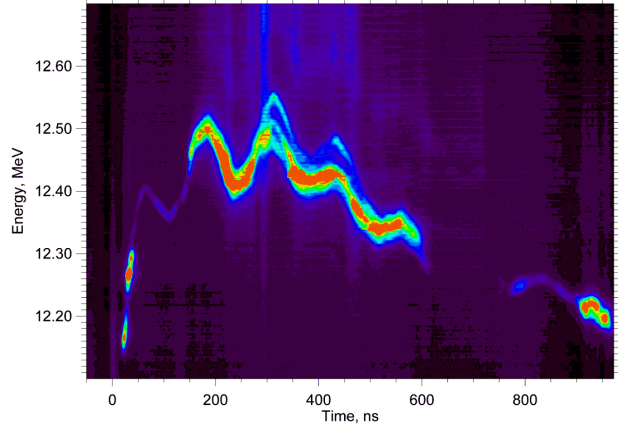

Figure 9. Streak camera readout of electron energy during an un-crowbarred pulse.

Spectrometer measurements of beam energy after the eight injector cells gave a peak of 4.2 MeV. The diode A-K potential was 3.0 MV, so these measurements indicate an average beam-loaded accelerating potential of 150 kV/cell for the injector and 136 kV/cell for the 61 active standard cells.

Anamorphic streak images (Fig. 10) of the beam after the accelerator exit showed that the elliptical beam profile had a Gaussian-like core surrounded by a halo.(Fig. 11) that includes <20% of the total current. The beam centroid motion seen in the streak images has excellent correlation with the beam position measured with a BPM 40 cm upstream of the imaging target.
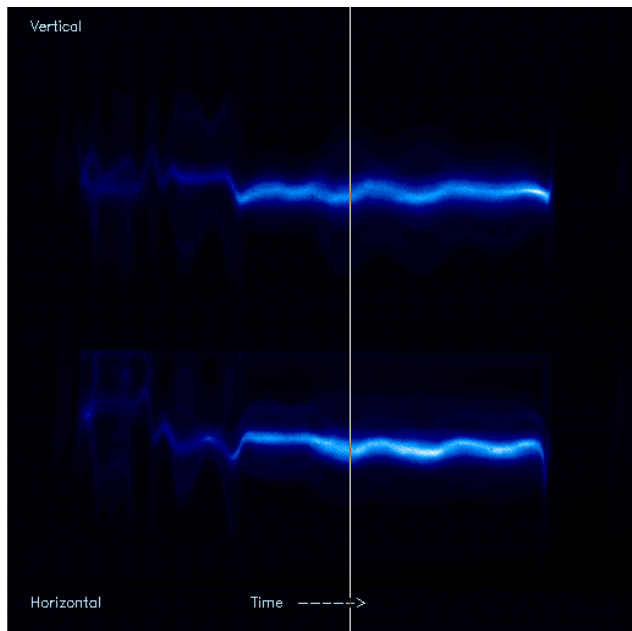

Figure 10. 1.0-μs anamorphic streak images of ~1.5-cm diameter beam. Top: Projection in vertical plane (anamorphically compressed in horizontal direction). Bottom: Projection in horizontal plane(anamorphically compressed in vertical direction). Time runs left to right.
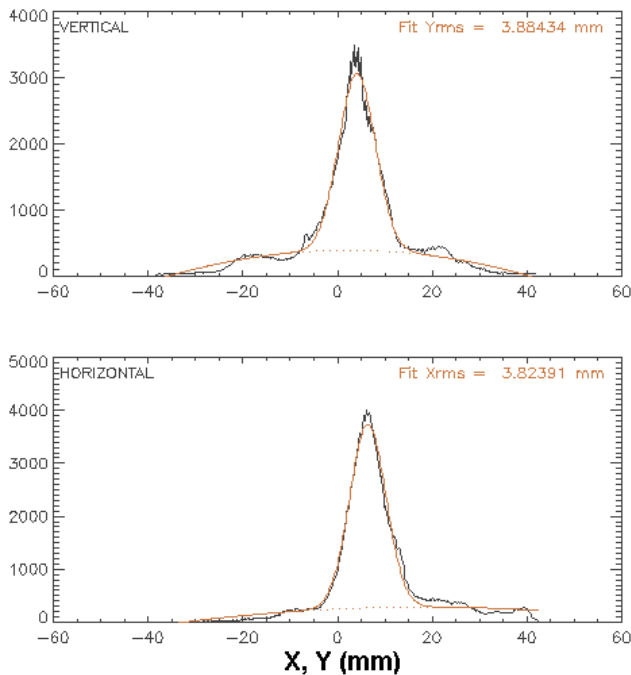
Figure 11. Projections at lineout time shown in Fig. 10. A fitted model consisting of a Gaussian core plus quadratic halo is over-plotted. Amplitude units are raw CCD counts.

Target heating is an issue for long-pulse beam imaging. If the imaging target gets too hot, evolved gas is ionized by electron impact, and ions are accelerated into the beam by the beam space charge, partially neutralizing it. This causes ion focusing of the beam, or even disruption [6], either of which invalidates the imaging data. The threshold for these effects is over 300C [7]. We estimated the temperature of the target by time-integrating movies of maximum-entropy reconstructions of the beam current density profile to get maps of charge deposition, and then temperature using stopping power and specific heat. We concluded that imaging data near the peak current, but shortly after the risetime, were likely free of confusing ion effects.

To estimate the beam emittance we changed the focal point on several consecutive shots using one of the solenoids after the accelerator exit. We then found the most likely emittance at the accelerator exit by fitting the profile size as a function of focus magnet strength with the XTR envelope code predictions [4,8]. The normalized Lapostolle emittance (4rms) was > 4000 π-mm-mr because of the halo (Fig. 11). On the other hand, had we scraped off the halo with an aperture, the emittance of the remaining beam core (~80% of total current) would have been < 1000 π-mm-mr.

We concluded this first round of commissioning with tests of resistance to BBU. No evidence of BBU growth was seen until the magnetic field strength was reduced by a factor of 5 throughout the 64 standard cells. Figure 12 shows a wavelet frequency analysis of the motion of the beam centroid, dX/dt, derived from un-integrated BPM signals near the end of the accelerator. On this shot with 20% field motion in the BBU frequency band is seen to grow at late times. This result verifies the robustness of this tune to BBU and implies BBU will be suppressed when we begin operations with the final 2-kA beam current.
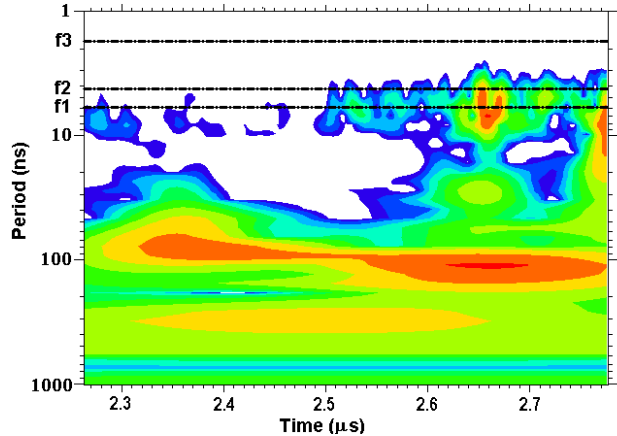

Figure 12. Frequency analysis of motion of the beam centroid with magnetic field reduced by factor of 5. BBU frequencies for the accelerator cells are f1=169 MHz, f2=236 MHz, and f3=572 MHz [9].

ACKNOWLEDGEMENTS

REFERENCES

[1] "Status of the DARHT Phase 2 Long-Pulse Accelerator," M. J. Burns, et. al., PAC2001, Chicago, IL, June 2001, p. 325

[2] "Beamline tunes for DARHT-II phase-1 commissioning," Carl Ekdahl, Los Alamos National Laboratory report LAUR-02-3921, June 27, 2002

[3] "Finite-element Methods for Electron Gun Design," Stanley Humphries Jr., ICOPS'96, and www.fieldp.com

[4] "Beam injector and transport calculations for ITS," Thomas P. Hughes, David C. Moir and Paul W. Allison, PAC'95

[5] "Fourier-analyzing coil arrays for pulsed relativistic electron beam experiments," C. A. Ekdahl, Rev. Sci. Instrum. 55, 1221 (1984)

[6] "Effect of target-emitted ions on the focal spot of an intense electron beam," Dale R. Welch and Thomas P. Hughes, Lasers and Charged Particle Beams 16, 285 (1998)

[7] "Ion emission from solid surfaces induced by intense electron beam impact ." C. Vermare, H. A Davis, D. C. Moir, and T. P. Hughes, Phys. Plasmas 10, 277 (2003)

[8] "Reconstruction of initial beam conditions at the exit of the DARHT II accelerator," A.C. Paul, LINAC2000, Monterey, CA, August 2000, p. 455

[9] "BBU and Corkscrew Growth Predictions for the DARHT Second Axis Accelerator," Y. J. Chen and W. M. Fawley, PAC2001, Chicago, IL, June 2001, p. 3490